Original Paper

A Trapezoidal Three-Dimensional Model for Gas Extraction Based on Shapes of Caved Overlying Strata and Numerical Calculation

Pan Wei ⓘ,[1,2] Xuelong Li,[1,3] Qianting Hu,[1,4] Shoujian Peng,[1,4] and Shu Liu[1]

Gas emission from the working face in a gas-bearing coal seam impairs safe production. Especially in the coal face, influenced by mining, pressure-relief gas in adjacent seams flows into the working face through the goaf. Moreover, caved overlying strata in different regions show differences in pore and seepage characteristics. Thus, the caving of overlying strata in the goaf of a working face was explored by carrying out physical similarity simulation. Then, based on the characteristics of the geometric shapes of caved overlying strata after mining, a trapezoidal three-dimensional model for gas extraction was established. According to the calculation result, the parameters of field high-level boreholes were optimized. Then, the controllability of gas concentration at the working face after gas extraction was assessed by applying statistical process control. The result showed that after the observed surface of the physical similarity model was lightened, it was more favorable for conducting the test. Moreover, the maximum gas concentration in the goaf was negatively correlated with the diameter of high-level boreholes and the negative pressure for gas extraction. A statistical process control chart revealed that the gas concentrations at the working face were safe after gas extraction based on high-level boreholes, which also validated the feasibility and effectiveness of the model.

KEY WORDS: Coalbed methane, Physical similarity simulation, Numerical simulation, Trapezoidal three-dimensional (3D) model, Extraction parameters, Statistical process control (SPC).

INTRODUCTION

With the constant and rapid growth of China's economy, the demand for coal, petroleum, and nat-

[1]State Key Laboratory of Coal Mine Disaster Dynamics and Control, School of Resources and Safety Engineering, Chongqing University, Chongqing 400044, China.
[2]Institute of Mining, Clausthal University of Technology, 38678 Clausthal-Zellerfeld, Germany.
[3]Henan Key Laboratory for Green and Efficient Mining and Comprehensive Utilization of Mineral Resources, Henan Polytechnic University, Jiaozuo 454000, Henan, China.
[4]To whom correspondence should be addressed; e-mail: 20172001029@cqu.edu.cn, sjpeng@cqu.edu.cn

ural gas is increasing; however, due to the characteristics (rich in coal, less rich in petroleum, and with lean gas reserves) of the energy structure of China, an energy consumption structure centered on coal has developed (Fan and Xia 2012; Lau et al. 2017). In recent years, affected by environmental pollution and other factors, China also has developed other clean energy sources such as wind energy, solar energy, and natural gas hydrates. However, clean energy is far from meeting China's demand; therefore, coal resources still exert strategic significance on China's economic development (Chen 2005; Wang et al. 2012b; Chen et al. 2016).

Under China's heavy demand for coal, coal seams having a large burial depth, under complex geological conditions, and at risk of disaster, now have to be mined. This makes Chinese coal expensive. During 2007–2017, China's coal mines were subjected to 354 gas accidents, causing 2655 deaths. The number of gas accidents accounted for about 45% of the total number of coal mine accidents and the death toll in gas accidents accounted for over 40% of those in coal mine accidents (Fig. 1) (Chen et al. 2012; Wang et al. 2014; Yin et al. 2017). Gas in mines is regarded as the first fatal factor, and it has dual characteristics: It is a greenhouse gas, with greenhouse effect being more than 20 times higher than CO_2. This methane is also a source of clean energy; therefore, it is necessary to eliminate the threat of gas disasters occurring in mines and further utilize the gas (Karacan et al. 2011; Hu et al. 2017; Wang et al. 2019b).

At present, gas extraction is taken as the primary measure for gas prevention and control (Xu et al. 2017; Wei et al. 2019a, b, c). After considering the greenhouse effect of gas, China also transforms the act of *gas drainage* into *gas extraction*. Engineering practice shows that with the mining of coal face, coal seams and strata are caved and broken to further generate more fractures. The pressure-relief gas released from the residual coal of adjacent seams and goaf tends to flow into the working face under the effect of negative pressure during ventilation, causing gas concentrations at the upper corner to exceed safe limits. Currently, the pressure-relief gas of goaf in China's mines is governed mainly through gas extraction based on high-level boreholes (GEHLB), gas extraction based on high-level suction roadways, gas extraction through surface 1000-m drilling rigs, gas extraction based on underground 1000-m drilling rigs, and the mining of protective seams. Compared with other methods, GEHLB is more mature and easier to implement; additionally, it is easier to distribute and adjust high-level boreholes according to in situ conditions (Wang et al. 2012a, b; Hou et al. 2012; Hu et al. 2015; Qu et al. 2015; Li et al. 2015; Zhou et al. 2016; Liu et al. 2017; Wang et al. 2017, 2019a, 2020).

Analysis shows that, when the optimal location of the bottoms of high-level boreholes is found at the mid-lower part of a fractured zone, the optimal extraction efficiency based on high-level boreholes can be realized (Qu et al. 2015; Wang et al. 2019b). Therefore, high-level boreholes are distributed on the basis of the characteristic geometry of caved overlying strata in goaf. Based on the Voussoir beam theory, the concepts of three horizontal zones (including impact area of coal wall support, bed-separated, and re-compacted regions) and three vertical zones (including a caved zone, a fractured zone, and a bent zone) are proposed based on the migration of overlying strata after mining (Qian et al. 1996; Karacan et al. 2007; Li et al. 2011). As shown in Fig. 2, the overlying strata are divided into a caved zone, a fractured zone, and a bent subsidence zone from bottom to top in the working face according to the strata migration. The practice result showed that the lithology of overlying strata affects the migration, deformation, and fracturing of strata. It has been revealed that there are three different moving zones after mining overlying strata along the longwall face (Palchik 2003; Keim et al. 2011; Majdi et al. 2012). Based on similarity simulation and field practice, Liu proposed the notion of three horizontal zones and three vertical zones (Zhang and Liu 1990; Liu 1995). By using various methods including model experiment, image analysis, and discrete element simulation, Xu et al. (2004a, b) revealed the two-phase development of fractures induced by mining overlying strata in a longwall face and the distribution thereof was circular. Li et al. (2014) divided the mining-induced fracture field into the fracture field above the working face and that above the goaf and revealed the dynamic distribution characteristics of elliptic–parabolic fracture zone caused by the mining of overlying strata. Numerous scholars explored the caving of overlying strata in goaf by employing diverse methods including physical similarity simulation, UDEC, FLAC, and RFPA (Guo et al. 2017).

Additionally, after determining the distribution mode and location of high-level boreholes, these parameters (including borehole diameter, negative pressure during gas extraction, hole-sealing depth, and hole-sealing materials) are important when determining extraction yield. At present, the gas flow in goaf and the zone subject to gas extraction are analyzed by applying theoretical fluid mechanics, field observation, and numerical simulation method to determine the optimal extraction parameters (Zhang and Bian 2015; Guo et al. 2015; Zhou et al. 2016; Xu et al. 2017; Liu et al. 2019). From such analyses, a mathematical model for gas migration has been proposed from the perspective of the mechanism of gas flow in coal seams. Numerous scholars have investigated the flow of gas in goaf by using computational fluid dynamics (CFD) (Chu
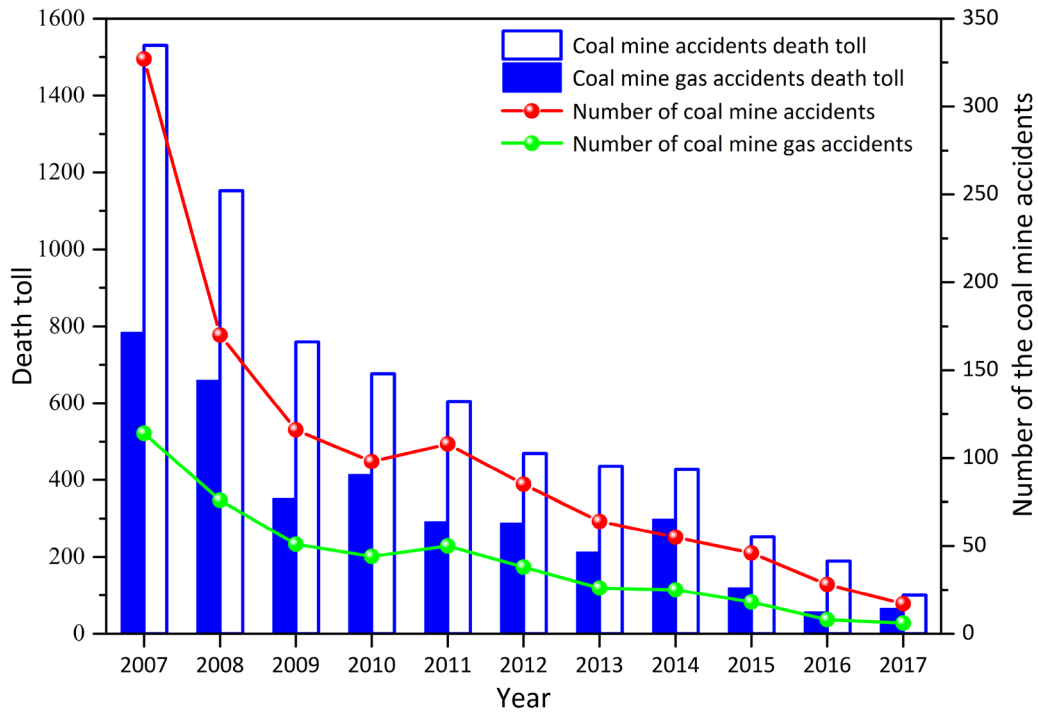
Figure 1. Statistics of coal mine accidents (2007–2017).
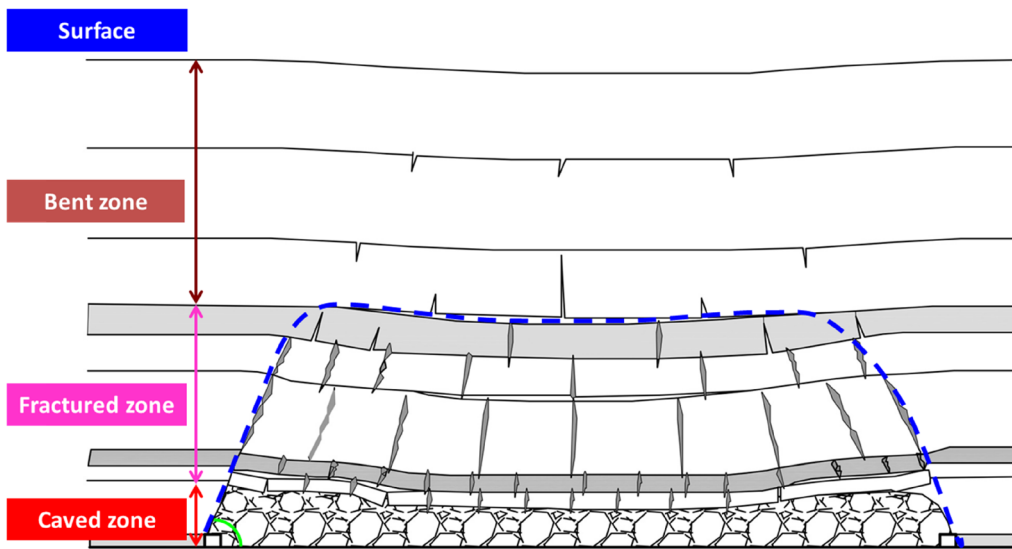

Figure 2. Division of overlying strata of working face and goaf.

et al. 2011; Guo et al. 2015; Qin et al. 2015). By applying CFD, Hu et al. (2007) simulated a gas flow under conditions of surface drilling for gas drainage. Cheng et al. (2016) and Brune and Saki (2017) ex-plored some problems, including gas migration in goaf and spontaneous combustion of coal in goaf, by using CFD. Somerton et al. (1975) studied the per-meability of cracked coal bodies under nitrogen and

methane gas under triaxial stress. Gawuga (1979), Khodot (1980), Harpalani (1985) and other scholars studied the mechanical properties of gas-bearing coal samples in the geophysical field and the solid–gas mechanics effects between coal rock mass and gas percolation. Borisenko (1985) studied the effective stress of coal body under the action of pore pressure from the perspective of the principle of pore area of coal body and solid area of solid skeleton. Enever and Hennig (1997) studied the interaction between permeability and effective stress of gas-bearing coal seams in Australia and concluded that the change in permeability of coal seams and the change in in situ stress are exponential. By introducing diffusion–translation equation for solute and Fick diffusion law, Li et al. (2012) simulated the flow and diffusion behaviors of gas. By using the Navier–Stokes (N–S) equation and Brinkman equation, a model for gas flow in the working face and goaf was established, and the physical model was solved by employing the COMSOL Multiphysics analysis tool for multiphysics coupling (Li et al. 2012). Scholars in China make model or program simulation software by themselves based on the seepage–diffusion law to explore the gas seepage field of coal seams and gas concentration field in mines from the perspectives of theory, experiment and field test data. For example, Li (2016) developed *Analysis Software for Gas Flow of Boreholes CO-MESS2.0* and conducted numerical simulation of gas emissions.

However, in terms of shape, the geometric models established by numerous scholars are cuboidal. The true shape of caved overlying strata after mining coal seams is not taken into account. Therefore, to reflect the distribution of gas in the mine, the caving of overlying strata in goaf after mining the coal seams was analyzed by conducting physical similarity simulation tests based on field conditions. On this basis, a trapezoidal three-dimensional (3D) model for GEHLB was established through ANSYS Fluent to simulate the distribution law of gas concentration on different extraction conditions. In this way, the optimal extraction parameters for high-level boreholes are obtained. The media within the goaf are made of solid frameworks, and a great number of densely distributed tiny pores are formed and separated by the framework, which contains rock with pores and fractures, characterized as being multiphase, with defined pore properties and connectivity. Therefore, the trapezoidal 3D model for GEHLB based on the caving of overlying strata in goaf established according to different pore characteristics of the three zones conforms more closely to the actual condition of the minefield in shape. Moreover, the model is more favorable when showing the differences in seepage characteristics of the three zones. Therefore, the calculated result is more consistent with actual field conditions.

ENGINEERING BACKGROUND

The coal-bearing strata in the well field used for the test are Upper Carboniferous Taiyuan formation and Lower Permian Shanxi formation, containing 12 coal seams, in which the No. 5 coal seam is minable. The upper No. 4 coal seam adjacent to the No. 5 coal seam was 5 m from the latter, with an average thickness of 1.2 m. Other coal seams were unworkable and were sparsely distributed within the well field and far from the No. 5 coal seam. The working face for the test was firstly mined in the mine, in which the No. 5 coal seam was primarily mined, with the thickness of the coal seam being 0.40–10.54 m, with an average thickness of 4.0 m, a bulk density of 1.4 t/m³, and a mean dip angle of 3°. The working face was mined by using retreating mining, and the whole thickness of the seam was mined at once through fully mechanized mining. Moreover, caving coal mining method was applied to control the whole roof of the coal seams. The strike length of the working face was 2500 m, while the length was 150 m in the direction of trend. The amount of air distribution was designed to be 1000 m³/min. (The gas discharge via ventilation was 8 m³/min.)

The mine for the test was located in new mining area, and the mined No. 5 coal seam was a typical soft coal seam with soft roof and floor. (The mechanical parameters of rock samples at the roof and floor are listed in Table 1.) Moreover, the coal seams in the test working face had high gas content, and therefore the basic parameters of gas in coal seams were measured before mining (Table 2). Moreover, according to different-source prediction method (Wei et al. 2019a, b, c), the amount of gas emitted from the working face was predicted and is expected to provide a basis for preventing and controlling gas at the working face.

Table 1. Test results of coal and rock mechanical parameters

Type of strata	Tensile strength (MPa)	Compressive strength (MPa)	Elastic modulus (GPa)	Cohesion (MPa)	Internal friction angle (°)	Poisson's ratio
Roof	1.382	23.351	24.162	5.86	29.81	0.264
No. 5 coal seam	0.641	6.213	9.867	2.21	24.66	0.286
Floor	1.421	21.768	20.198	5.74	28.88	0.288

Table 2. Basic parameters of gas in coal seams

Gas content (m^3/t)	Attenuation coefficient of gas flow in boreholes (d^{-1})	Protodyakonov coefficient	Adsorption constant		Industrial analysis		
			a (cm^3/g)	b (Mpa^{-1})	$M_{ad}/\%$	$A_{ad}/\%$	$V_{daf}/\%$
3.07	0.807	0.5411	17.37	1.51	0.66	34.58	23.17

When the daily yield of the working face was set to 7000 t/d, the amount of gas emitted from the working face was 11.122 m^3/min. Discharging gas by ventilation alone cannot satisfy safety requirements (8 m^3/min < 11.122 m^3/min), so it was necessary to take preventative measures. Additionally, according to Temporary Provision of Gas Drainage Reaching Standard in Coalmine (No. 163 document of State Administration of Work Safety for Coal Devices, 2011), it was essential to conduct gas extraction when the amount of gas emission in the coal face exceeded 5 m^3/min. Thus, preventative measures for gas pre-extraction in the coal seam were taken in the test working face; however, after gas pre-extraction, gas concentrations still exceeded the limit during the mining of the working face (especially in the upper corner). Through analysis, the reason was that the attenuation coefficient of gas flow of the boreholes in the No. 5 coal seam was 0.807 d^{-1}, which was larger than the critical value (0.05 d^{-1}), at which gas extraction was difficult. As a result, the gas pre-extraction effect of the coal seam was undesirable. Moreover, the No. 4 coal seam was close to the No. 5 coal seam and was also thick; therefore, after mining the No. 5 coal seam, the overlying strata in the mine field were caved and then pressure-relief gas in the No. 4 coal seam and the gas released from the residual coal in goaf flowed into the working face, causing high gas concentrations in the upper corner. After learning from the preventative measures for gas in adjacent coal mines, the pressure-relief gas in goaf in the coal mine was extracted through high-level boreholes.

PHYSICAL SIMILARITY SIMULATION EXPERIMENT

Design of Excavation Model and Excavation Method

Determination of Similarity Constant

In the similarity simulation, the basic properties and similar characteristics of similar phenomena were described by using three similarity theorems based on similarity theory. Various important physico-mechanical parameters (including geometry, motion, dynamics, and boundary conditions) of the model are similar to those of the prototype. The similarity constants of the test model were selected according to the test requirement, and those of stress and strength were determined according to similarity theorems. The similarity constants of the model are listed in Table 3.

Model Design

In terms of model design, a 2D planar model was established according to the engineering conditions at the test working face (see ''Engineering

Table 3. Similarity constants of the test model

Dimension of framework of the model (mm × mm × mm)	Similarity constant					
	Geometry α_L	Time α_t	Bulk density α_γ	Poisson's ratio α_μ	Stress α_σ	Strength α_E
3000 × 200 × 1300	100	10	1.5	1.0	150	150

Background'' section). The section of the working face along the strike was excavated and simulated along the coal seam. The strike length and average mining height of the working face designed in the model were 3 m and 0.04 m, and the height of the model was 1.2 m. Moreover, the other overlying strata were loaded through gravity compensation.

Material Ratio of the Model

Based on the comprehensive columnar section and lithological and mechanical parameters of the test working face, the material ratio of the model was calculated (Table 4). In the test, fine sand was used as the aggregate and gypsum and talcum powder were used as cementing agents. Moreover, mica was used to simulate primary stratification. During construction of the model, it was guaranteed that the materials were uniformly mixed and a 1-cm layer of bed rock was laid, in which joints and stratifications were set. After the model was built, favorable ventilation conditions in laboratory were maintained so that the model was dried to reach the test requirements for excavation.

Test Method

To explore the migration of overlying strata and evolution of fractures in the mine field, the following steps were followed.

(1) By using talcum powder and a gypsum–water solution, the observed surface was uniformly whitened to allow observation of the development of fractures.
(2) Pressure sensors were set at the bottom of the model to record the pressure on the mine field during the mining of coal seams.
(3) The test phenomena and development conditions of fractures were photographed using a digital camera and measured using a steel ruler.

Excavation Scheme During the Test

After the model has satisfied the mining conditions, the observed surface of the model was whitened (Fig. 3). After the surface of the model was dried, the excavation step distance and time interval were calculated according to the ratio of geometric similarity and time similarity constants. Moreover, a 30-cm-thick coal pillar was separately left at the left- and right-hand sides of the model, with the size of the open-off cut of 80 mm. The mining height of the model was 40 mm, while 20 mm of coal seam was excavated each time. After each excavation step, coal samples were photographed to record related parameters after the strata were caved and then stabilized.

The Excavation and Its Analysis

Development of Fractures and Related Analysis

During the test, the development conditions of fractures after the excavation can be clearly observed. Additionally, it can be found that overlying strata successively showed bed separation, subsidence, and fracturing. The direct reason why overlying strata of the mine field were subjected to a large area of movement, deformation, and fracture was that the transverse and longitudinal fractures induced by mining were connected. Therefore, it was feasible to discriminate whether overlying strata were fractured or caved according to the observed development conditions of bed-separated fractures and longitudinal fractures.

After whitening the observed surface of the model, the development and coalescence of fractures during the excavation can be found (Fig. 4). Therefore, judging whether overlying strata will be fractured or caved according to the observed development of transverse (Fig. 4a) and longitudinal (Fig. 4b) fractures was more favorable to conducting the test. When mining the soft coal seam with a soft roof and floor that was rich in gas, the strength of

Table 4. The material ratio of the test model

Serial number	Layer	Thickness of model (cm)	Sand (kg)	Gypsum (kg)	Talcum powder (kg)	Coal ash (kg)
1	No. 5 coal seam	4	4.239	0.188	0.754	4.239
2	Mudstone	3	8.243	0.471	0.707	
3	Sandy mudstone	2	8.373	0.419	0.628	
4	Fine sandstone	2	8.243	0.471	0.707	
5	No. 4 coal seam	1	4.239	0.188	0.754	4.239
6	Sandy mudstone	17	8.373	0.419	0.628	
7	Siltstone	4	8.243	0.236	0.942	
8	Sandy mudstone	9	8.373	0.419	0.628	
9	Medium sandstone	5	8.243	0.353	0.824	
10	Siltstone	12	8.243	0.236	0.942	
11	Sandy mudstone	14	8.373	0.419	0.628	
12	Fine sandstone	7	8.243	0.471	0.707	
13	Sandy mudstone	4	8.373	0.419	0.628	
14	Siltstone	20	8.243	0.236	0.942	
15	Sandy mudstone	26	8.373	0.419	0.628	
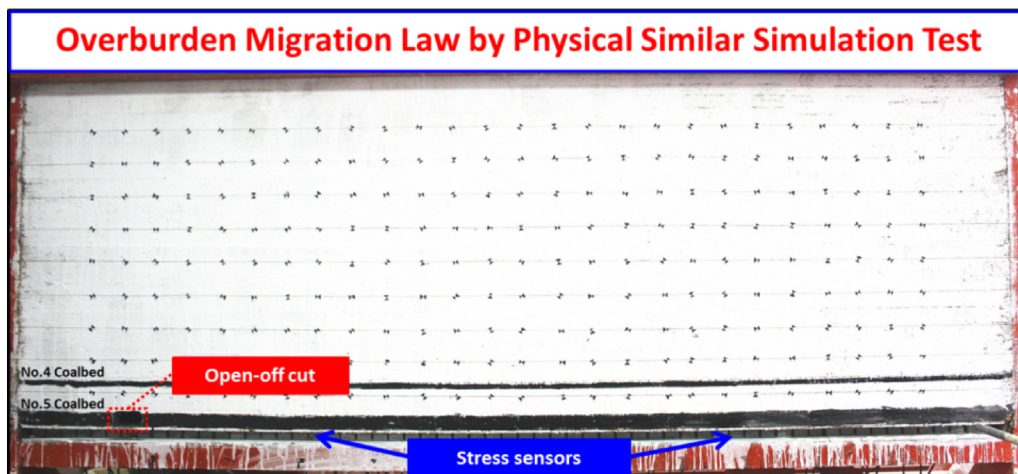
Figure 3. Construction of the model.

coal seams was low and therefore the change in external conditions exerted a greater influence on gas migration compared with general coal seams. The distribution of the three zones of overlying strata was considered important when investigating gas migration and accumulation. Additionally, it was necessary to explore the dynamic changes in the caving of overlying strata and the height of bed separation after mining the soft coal seams with soft roof and floor to analyze the migration and accumulation shapes of gas in the fracture zone. When mining coal seams, the strata were subjected to deformation, migration, fracturing, and caving during mining; thus, bed-separated fractures and breaking fractures were found in the overlying strata and developed upwards with the advance of each layer.

Figure 5 shows the relationships of the highest location of fractures and the caving height with the advancing distance of the working face: Breaking fractures were generated later than the bed-separated fractures. When the open-off cut was formed, bed-separated fractures were generated at the immediate roof. After the first periodic weighting appeared in the working face, the caving rate of overlying strata increased and a significant caving event occurred every 4–8 m. The development of bed-separated fractures was not completely syn-
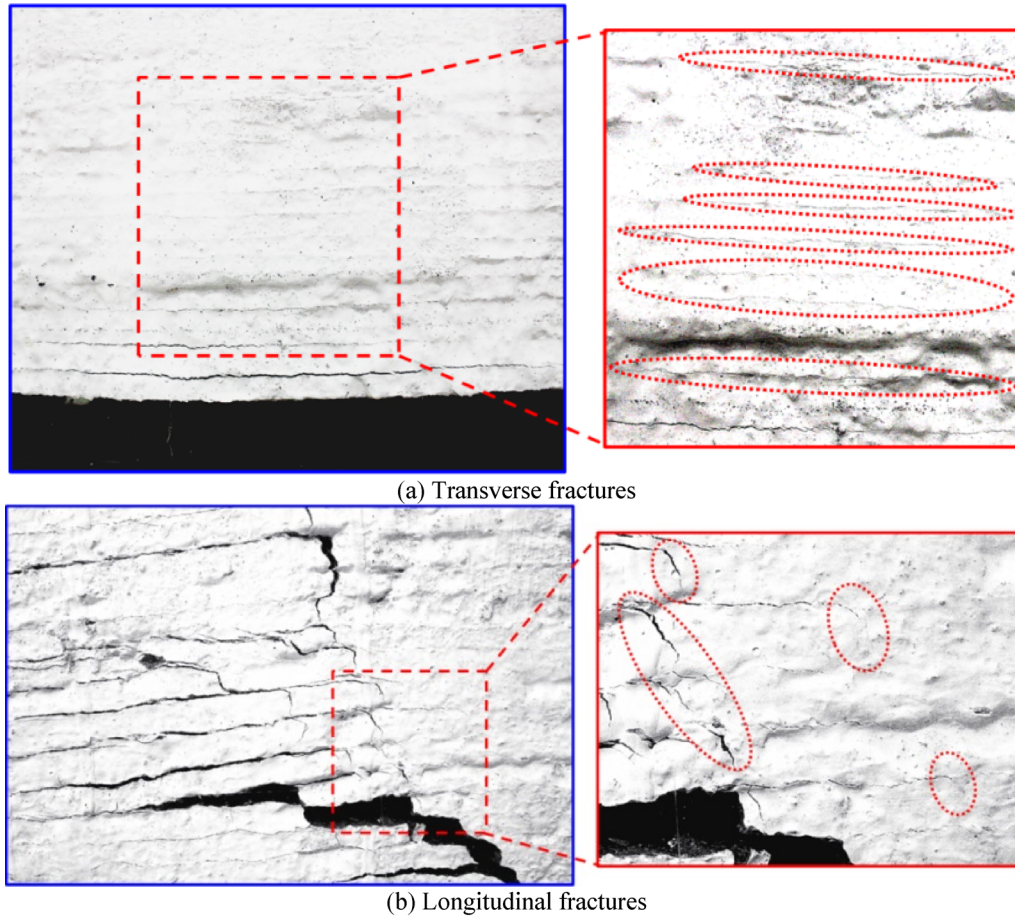
(a) Transverse fractures

(b) Longitudinal fractures

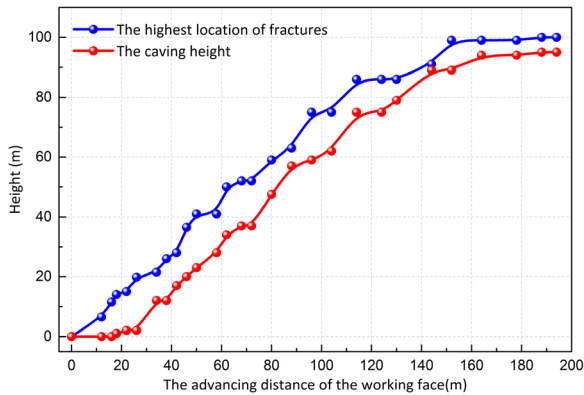**Figure 4.** Fracture development conditions during mining.

Figure 5. Relationships of the highest location of fractures and caving height with advancing distance of working face.

chronous with that of breaking fractures: The bed-separated fractures developed faster than breaking fractures. When the two types of fractures extended upwards, the extension of fractures ceased when inferior key strata appeared. With the advance of the working face, the bed-separated zone expanded and bed separation did not continue to extend upwards before the inferior key strata were fractured; however, the bed separation did not develop upwards after they extended to the key strata.

According to the test result by using the model along the strike, it can be seen that the breaking fractures were developed 17–29 m from the floor of the coal seams and the bed-separated fractures were found in the zone below a depth of 110 m. Between 95 and 110 m, the bed-separated overlying strata were bent. After the working face advanced to 152 m, the bed-separated fractures and breaking fractures changed slightly, while they were closed when the working face was subjected to sixth and 13th periodic weightings after being advanced to 80 and 144 m. Afterwards, caving was insignificant over a long advancing distance.

Analysis of Caving of Strata

During excavation, the bed-separated fractures constantly expanded after the working face was advanced to 22 m; after being advanced to 26 m, the strata at the upper main roof reached the limit and therefore main roof fractured and sank, causing a large area of the roof to fall. Therefore, the first weighting appeared in the working face and bed-separated fractures were found in the zone some 19.8 m from the roof of the coal seam. Moreover, the height of the cavity was 4 m and the width of rock beam was 15.5 m, as shown in Fig. 6a. When the working face was advanced to 88 m, the eighth periodic weighting occurred to the working face. In this case, the fractures were closed and goaf was gradually compacted. The bed-separated and breaking fractures developed in the zones 75 m and 59 m away from the roof of the coal seam, respectively (Fig. 6b).

After the eighth periodic weighting, the overlying strata in goaf were stable. A periodic weighting

appeared once the working face was advanced by 6–14 m, with an average weighting span of 8 m. The small weighting span was caused by the characteristics of soft coal seams with a soft roof and floor: The coal seams and strata at the roof and floor exhibited poor mechanical properties and low tensile and shear strengths. As a result, strata were easily fractured and tended not to form a hinged structure. Accordingly, it can be seen that the caved strata in the caving zone of the soft coal seams with soft roof and floor were broken and fractures were more developed. Moreover, the first and periodic weighting spans of the working face were less significant.

After the working face was advanced to 194 m, the partition of zones with fractures in the mine field is shown in Fig. 7. Then, the mining and caving in the mine field were completed and stabilized. By analyzing the comprehensive columnar section of coal seams in the working face and strengths of various strata, the characteristics of geometric shapes of caved overlying strata in the working face of the mine field can be attained. Moreover, the maximum height of the caving zone was 16 m and the breaking angle was 63°. Based on these, a trapezoidal 3D model for gas migration was established, as explained below.

SIMULATION OF GAS MIGRATION BASED ON A TRAPEZOIDAL 3D MODEL

The media within the goaf are made of a solid framework and many densely distributed tiny pores formed and separated by the framework, which contain numerous rocks with pores and fractures, characterized by being multiphase, with certain pore properties and connectivity. Therefore, the trapezoidal 3D model for gas migration based on the migration and evolution of fractures in overlying strata in the mine field was established according to different pore characteristics of the three zones to conform to in situ conditions. Moreover, the model better represents differences in seepage characteristics of the three zones.

Mathematical Model for Gas Seepage in Goaf

When conducting numerical simulation on flow field within the goaf, the flow field conforms to laws of conservation of mass, energy, and momentum. On
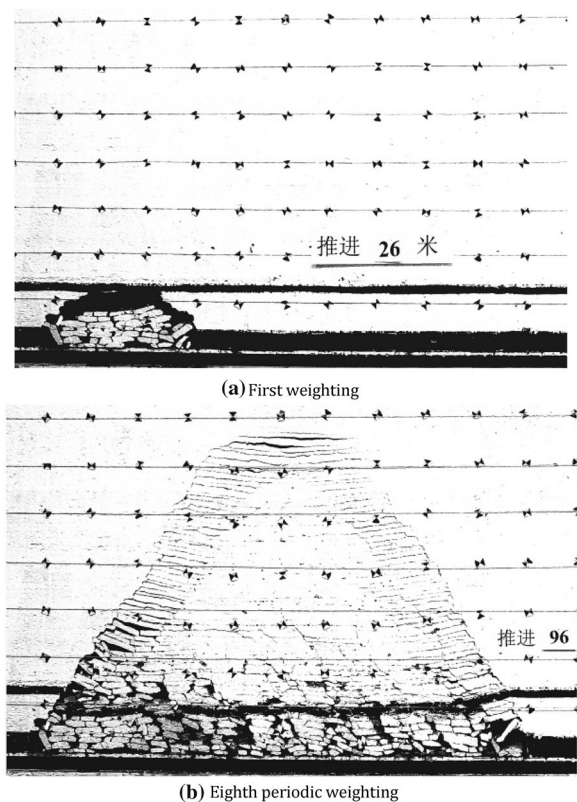

(a) First weighting

(b) Eighth periodic weighting

Figure 6. Caved overlying strata in mine field during periodic weighting.
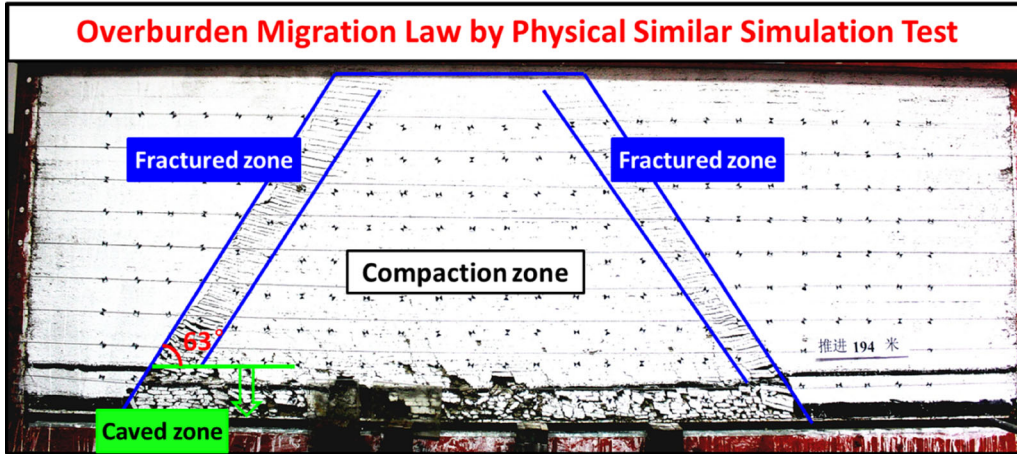
Figure 7. Partition of zones with fractures after working face was advanced to 194 m.

condition that the fluid flow is turbulent, the fluid system complies with turbulence equations. The conditions in goaf are complex, and there are many factors influencing the gas and spontaneous combustion of coal therein; thus, the following assumptions are made (Lin et al. 2016):

(1) The gas in goaf is considered incompressible and ideal; flow within the goaf conforms to seepage conditions. Only pure components of gas flowing into goaf are taken into account.
(2) The coal–rock mass in goaf is heterogeneous and porous.
(3) The permeability and porosity of goaf are subordinated to space functions but are not time-dependent.
(4) The oxygen uptake rate of residual coal in goaf is proportional to the oxygen concentration.
(5) The non-uniformity of gas concentration in goaf leads to gas diffusion, and the diffusion process is Fickian.

The interior of goaf contains mixed gas, including O_2, N_2, CO, CO_2, and CH_4, which all show mass exchange, that is, each component conforms to the law of conservation of mass. The mass conservation equation for active seepage is (Hu et al. 2008):

$$\frac{\partial(\varphi\rho)}{\partial t} + \nabla \cdot (\rho \cdot v) = q\rho \qquad (1)$$

Where φ, ρ, t, q, and υ refer to the porosity of porous media, gas density, time, strength of gas source, and the velocity of gas seepage, respectively.

At present, the standard k–ε mode is widely used, which incorporates the equation for turbulent dissipation rate ε based on the equation for turbulent kinetic energy k. The equation for k and the equation for turbulent dissipation rate ε in k–ε model are, respectively:

$$\frac{\partial(\rho k)}{\partial t} + \frac{\partial(\rho k u_i)}{\partial x_i} = \frac{\partial}{\partial x_j}\left[\left(\mu + \frac{\mu_t}{\sigma_k}\right)\frac{\partial k}{\partial x_j}\right] + G_k + G_b$$
$$- \rho\varepsilon - Y_m + S_k$$
$$(2)$$

$$\frac{\partial(\rho\varepsilon)}{\partial t} + \frac{\partial(\rho\varepsilon\mu_i)}{\partial x_i} = \frac{\partial}{\partial x_j}\left[\left(\mu + \frac{\mu_\tau}{\sigma_\varepsilon}\right)\frac{\partial\varepsilon}{\partial x_j}\right] + C_{1\varepsilon}\frac{\varepsilon}{k}(C_k$$
$$+ G_{3\varepsilon}G_b) - C_{2\varepsilon}\rho\frac{\varepsilon^2}{k} + S_\varepsilon$$
$$(3)$$

where σ_ε and σ_k denote turbulent Prandtl numbers of k and ε, respectively; $P_{rt} = \mu c_p/k_f$; G_k and G_b represent k generation terms for turbulent kinetic energy triggered by average velocity and buoyancy force, respectively; Y_m stands for the contribution of pulse expansion in compressible turbulence; $C_{1\varepsilon}$ and $C_{2\varepsilon}$ denote empirical constants; $G_{3\varepsilon}$ is a constant influenced by buoyancy force; S_ε and S_k represent the source terms; and k_f, μ, and μ_t denote the thermal conductivity coefficient, dynamic viscosity of gas in goaf, and velocity of turbulent flows, respectively.

Establishment of the Model

Model Development

The spacing between high-level boreholes drilled in the return airway was 50 m, and six high-level boreholes were distributed across each drill site, with a depth of about 90 m (adjusted according to field conditions). Furthermore, a trapezoidal 3D model for gas extraction on conditions of extracting gas via high-level boreholes was established (Fig. 8). The main body of the model is as follows: the length of the working face, depth of goaf, thickness of float coal, and heights of caved, fractured, and bent subsidence zones were 150, 200, 1.0, 16, 64, and 20 m, respectively; the roadway of the working face appeared as a rectangle, with a length of 4 m and width of 3.3 m. The X-, Z-, and Y-axes denote the direction from the intake airway to return airway of the working face, the direction upwards from the floor and the direction along the goaf, respectively.

Grid Generation

Grid generation is the basis of simulation, and the quality of grid generation determines the accuracy and precision of the analysis. Different parts of grids have different spacings. The roadway, working face, and float coal are regarded as a whole and were partitioned as hexahedrons, with the step length of 2 m. By using the cut cell method, grids were generated, with the maximum and the minimum of 3.2 m and 0.005 m, respectively. The number of elements is 917,050, and the partition result is displayed in Fig. 9.

Parameter Setting

The setting of boundary conditions is the key to solving the numerical problem. Setting reasonable conditions similar to the practical conditions is the premise of calculating more practical solution to flow field distribution. In the initial stage, goaf is in such an environment at a constant temperature and the flow of fluids is classed as seepage. No fluids flow on the wall surface of the coal, that is, the velocity is zero. The section of the working face remains unchanged, and the flow of gas is turbulent. The flow of gas in goaf is influenced by frictional resistance,

causing the variation of energy that is ΔP, which can be calculated as:

$$\Delta P = RQ^2 \qquad (4)$$

where R and Q refer to the ventilation resistance and ventilation rate in the working face, respectively. The other model parameters are summarized in Table 6.

Gas in practical goaf is generated from different sources, and it is impossible to clarify the amount of gas from different sources. Therefore, gas flowing out from only a single source is explored in the simulation process. According to the design of the test bed, gas in goaf flows uniformly from the float coal at the bottom of goaf during the simulation. During the numerical simulation, the gas in goaf flows from the residual coal of goaf, as an assumed uniform gas discharge. The amount of gas emissions was calculated, as explained above. Thus, the other parameters set in the model are listed in Table 5.

Simulation Result of Gas Migration on Conditions of GEHLB and Its Analysis

Without High-Level Boreholes Extraction

To analyze the extraction effect on conditions of GEHLB, the distribution of gas concentration of the working face when being not subjected to GEHLB was simulated (Fig. 10). In this way, it can be seen that the maximum gas concentration in goaf was 53.10%: The zones in goaf near the mine field and upper corner as well as the zone in return airway near the mine field all exhibited a high gas concentration that exceeded safe limits, conforming to in situ conditions; therefore, high-level boreholes are drilled to extract the pressure-relief gas in goaf to reduce gas emissions from the working face.

The diameter of boreholes and negative pressure of boreholes during GEHLB largely influence the extraction effect of high-level boreholes. Therefore, numerical analysis was carried out of gas emissions under conditions of gas extraction through high-level boreholes with different diameters and different negative pressures to determine the optimal diameter and negative pressure of high-level boreholes during gas extraction.
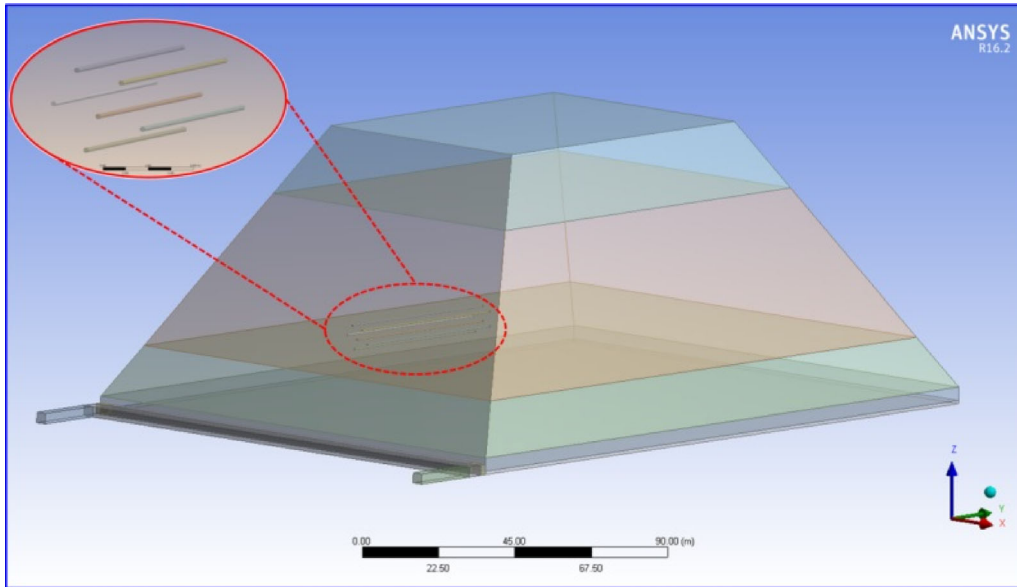
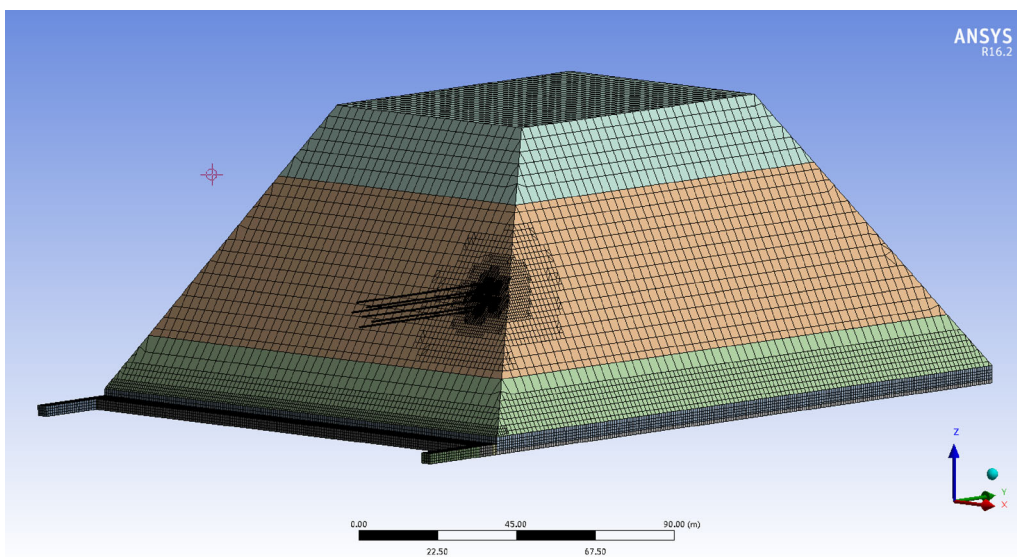**Figure 8.** Model for GEHLB.

Figure 9. Grid generation for the GEHLB model.

High-Level Boreholes Extraction with Different Diameters

The diameter of high-level boreholes affects the extraction effect to a large extent. Moreover, according to the special engineering background of the soft coal seams with soft roof and floor, the diameter of boreholes affects the stability of the boreholes. The high-level boreholes for gas extraction with five different diameters of 0.073, 0.089, 0.094, 0.113, and 0.153 m were drilled. Therefore, the gas concentrations under gas extraction through the boreholes with five different diameters were simulated to determine the optimal diameter of

Table 5. Parameter setting

Setting options	Setting mode (value)
Boundary of air inlet	Velocity inlet, intake airway with gas concentration of 0; air in air inlet, with the speed of 1.39 m/s
Boundary of air outlet	Boundary conditions of free outflow
Working face, roadway, and wall surface around goaf	No-slip boundary condition, that is, $u = v = 0$
Working face	Fluid region
Mining overburden strata in goaf	Zone with porous media
Float coal	User-defined function (UDF)
Source of gas emission	Float coal
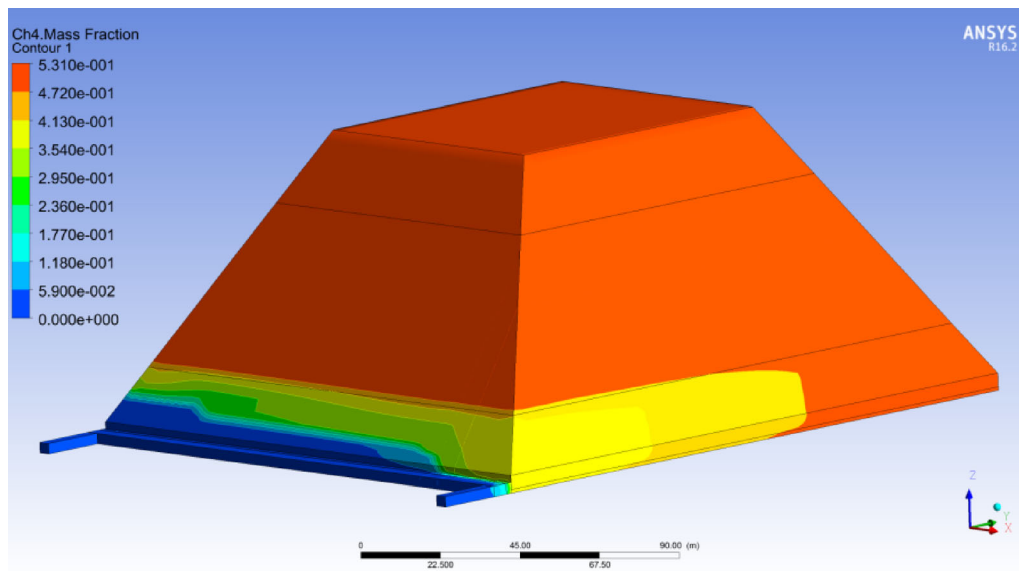
Figure 10. Distribution of gas concentration in goaf when gas extraction was not conducted.

boreholes. The simulated results of gas extraction through high-level boreholes with different diameters are shown in Fig. 11.

When the diameter of the high-level boreholes was 0.073 m (Fig. 11a), the maximum gas concentration in goaf was 59.19%. Compared with the result in Fig. 10 (i.e., without gas extraction), the maximum gas concentration in goaf slightly rose, while the zone with a high gas concentration shrank. The gas concentration in some areas reached 59.19%: Overall, the GEHLB has a little significant effect. When the diameter of high-level boreholes was 0.089 m (Fig. 11b), the maximum gas concentration in goaf was 40.26%, which was lower than

the result in Fig. 10. Compared with Fig. 11a, it can be seen that the zone with a high gas concentration further narrowed, implying that there was a more favorable extraction effect through boreholes with the diameter of 0.089 m. In the case that the diameter of high-level boreholes was 0.094 m (Fig. 11c), the gas concentration in goaf was no greater than 26.97%, which declined to about a half of the gas concentration when gas extraction was not conducted (cf. Fig 10). This indicated that the extraction effect was the optimal when the diameter of boreholes was 0.094 m, while the gas concentration at the upper corner of the working face remained high. When the diameter of high-level boreholes was
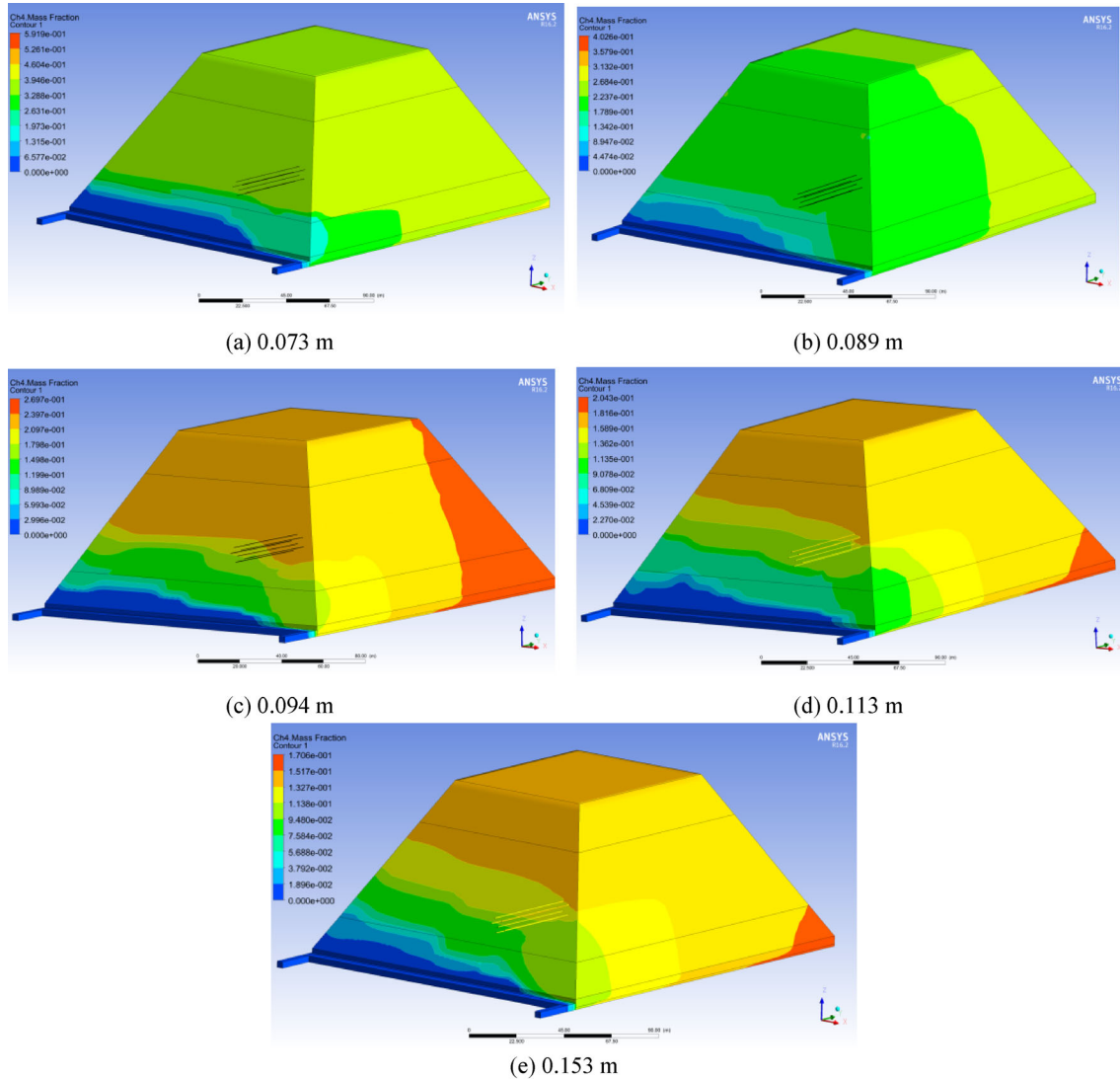
(a) 0.073 m

(b) 0.089 m

(c) 0.094 m

(d) 0.113 m

(e) 0.153 m

Figure 11. Nephogram of distribution of gas concentration in goaf when conducting gas extraction through high-level boreholes with different diameters.

0.113 m (Fig. 11d), the maximum gas concentration in goaf was 20.43%. After comparison with Fig. 10, it can be seen that the maximum gas concentration in goaf fell to less than half that without gas extraction: Moreover, gas in goaf converged into the high-level boreholes, indicating that the gas extraction effect was excellent. Additionally, the gas concentration in the upper corner decreased compared to the result shown in Fig. 11c. When the diameter of high-level boreholes was 0.153 m (Fig. 11e), the maximum gas concentration in goaf was 17.06% (less than a quarter of that before gas extraction).

Moreover, the gas in goaf flowed toward the high-level boreholes, evincing the efficacy of GEHLB. The gas concentration in the upper corner was safe, reaching the target set for gas extraction.

According to the simulation result, the relationship between the diameter of high-level boreholes and the maximum gas concentration in goaf is found (Fig. 12). The maximum gas concentration in goaf decreased with increasing borehole diameter. The only outlier in the figure appeared when the diameter of high-level boreholes was 0.073 m, at which the maximum gas concentration in goaf was
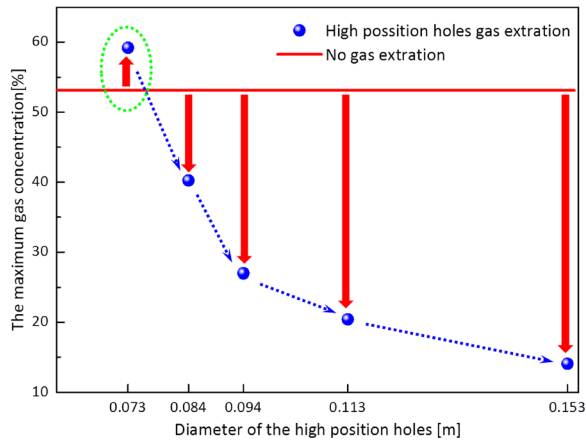
Figure 12. Relationship between borehole diameter and maximum gas concentration in goaf.

higher than that without gas extraction; however, on the whole, the gas concentrations in goaf decreased compared with those without gas extraction and the maximum gas concentration was found within a small zone in deep goaf.

Thus, the larger the diameter of high-level boreholes, the lower the gas concentration in goaf and the higher the extraction efficiency. However, along the path from the drill site to the borehole bottom, high-level boreholes successively crossed coal, overlying strata (caved zone), and the fractured zone. The porosities and shapes of fractures in coal–rock mass in different zones varied as did the mining-induced stress state. In a soft coal seams with a soft roof and floor, the size of high-level boreholes is restricted; therefore, based on the stability of boreholes in soft coal seams with soft roof and floor and construction conditions of boreholes in coal mine, gas extraction based on the high-level boreholes with a diameter of 0.153 m was applied to discharge pressure-relief gas.

High-Level Boreholes Extraction Under Different Negative Pressures

When the diameter of high-level boreholes was 0.153 m, the nephogram of distribution of gas concentration in goaf under four different negative pressures (5, 10, 15, and 20 kPa) during extraction was acquired (Fig. 13).

When the negative pressure of high-level boreholes during extraction was 5 kPa, the nephogram of gas concentration in goaf is shown in Fig. 13a. The maximum gas concentration in goaf was 21.17%, which decreased by 33.93% compared with that without gas extraction (Fig. 10). This indicated that the extraction effect was significant and the nephogram of distribution of gas concentration in goaf also changed significantly. In the case that the negative pressure of high-level boreholes during extraction was 10 kPa, the nephogram of gas concentration in goaf is as shown in Fig. 13b. The maximum gas concentration in goaf was 19.31%, which was reduced by 1.86% compared with the value at a negative pressure of 5 kPa during extraction. This implied that the extraction effect was unsatisfactory under increasing pressure. Under a negative pressure of 15 kPa during gas extraction via high-level boreholes, the nephogram of distribution of gas concentration in goaf is as shown in Fig. 13c. The gas concentration in goaf was no greater than 17.62% (a decline of 3.55% compared with that at a negative pressure of 5 kPa). However, in comparison with Fig. 13a, the morphology of the nephogram in Fig. 13c varied: High gas concentrations were found only in the deep goaf. At a negative pressure of 20 kPa, the nephogram of distribution of gas concentration in goaf is as shown in Fig. 13d. The maximum gas concentration in goaf was 14.06%, decreasing by 7.11% compared with the value at a negative pressure of 5 kPa. The gas concentration in the upper corner of the working face was under control, and the gas in goaf converged toward the high-level boreholes, indicating a favorable extraction effect. According to the morphology of the nephogram, the overall gas concentration in goaf at a negative pressure of 20 kPa decreased compared with that at 5 kPa. Compared with Fig. 13a, the nephogram of gas concentration changed significantly.

According to the simulation result, the relationship between the negative pressure during extraction through high-level boreholes and the maximum gas concentration in goaf is shown in Fig. 14. The maximum gas concentration in goaf decreased with the growth of negative pressure during extraction. This meant that the larger the negative pressure of high-level boreholes during extraction, the better the extraction effect; however, coal seams in the working face were classified as Type II seams prone to spontaneous combustion. When the negative pressure during extraction
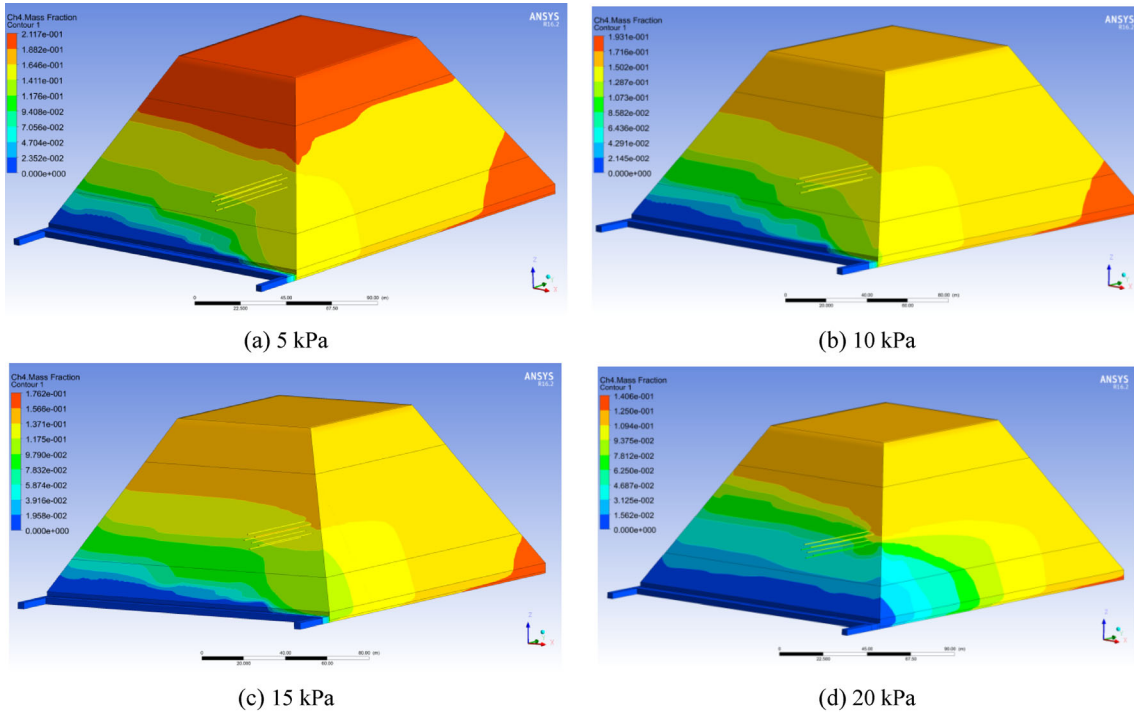
(a) 5 kPa

(b) 10 kPa

(c) 15 kPa

(d) 20 kPa

Figure 13. Distribution nephogram of gas concentration in goaf under different negative pressures during extraction.
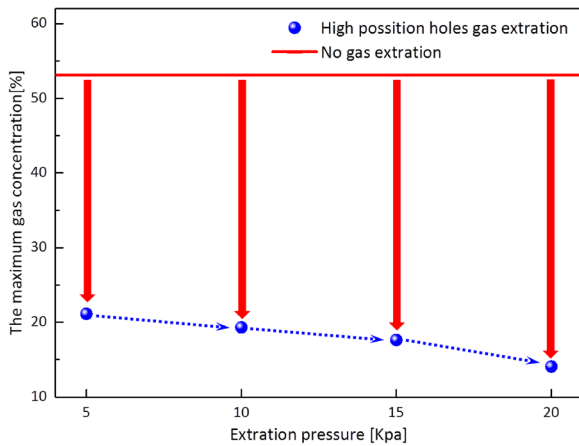

Figure 14. The relationship between the negative pressure in the boreholes during extraction and the maximum gas concentration in goaf.

reached 20 kPa, the gas extraction target can be realized. To prevent spontaneous combustion of residual coal in goaf during extraction under high negative pressures, and to reduce the load during extraction, it was not necessary to have a larger negative pressure during extraction. Therefore, a

negative pressure of 20 kPa was applied during extraction through high-level boreholes.

ENGINEERING APPLICATION AND EVALUATION OF EXTRACTION EFFECT

Engineering Application

Based on the results obtained through physical similarity simulation and numerical simulation, high-level boreholes are distributed (Fig. 15) according to conditions at the test working face. During extraction, 13 drill sites for gas extraction were set in the return airway, amounting to 78 high-level boreholes. The accumulated advance of boreholes during construction was 7121 m, and the gas concentration within the pipeline for gas drainage was between 2 and 42%. The amount of extracted pure gas was 1.29–9 m^3/min, and the total amount of extracted pressure-relief gas was 4.582×10^5 m^3.
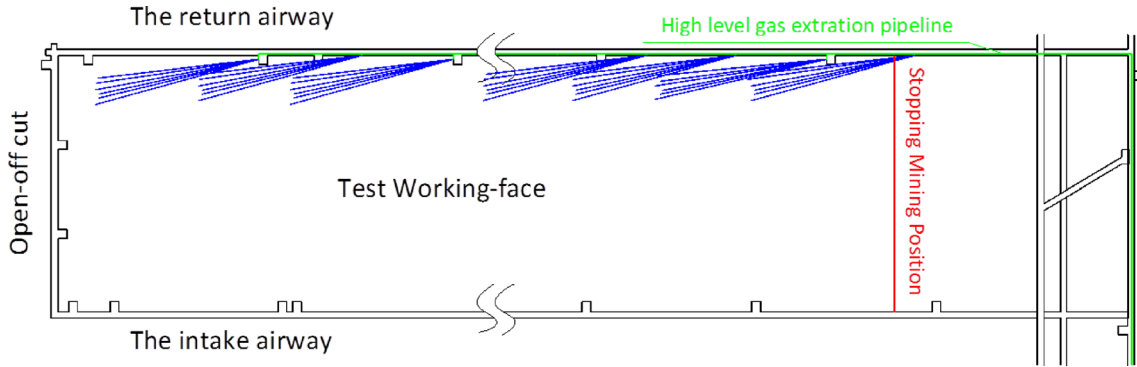
Figure 15. Distribution of high-level boreholes in the working face.

Assessment of Preventative Measures for Gas in the Working Face Based on SPC

SPC Chart

Statistical process control (SPC) was used to analyze a process and its output. The key to SPC is the control chart. Once abnormal data fluctuations are found, the reason for such an abnormality was analyzed and measures were taken to maintain the stability of a system (MacGregor and Kourti 1995; Bersimis et al. 2007).

The chart shows a central line (CL), indicating the mean of samples, upper control line (UCL), and lower control line (LCL) as well as plotted points of sequence of sample points extracted according to some time sequence. The range between the UCL and LCL was calculated using:

$$UCL = CL + 3\delta \tag{5}$$

$$LCL = CL - 3\delta \tag{6}$$

where CL and δ represent the mean and standard deviation of samples, respectively.

After taking preventative measures against gas accidents in the working face, once the gas concentration exceeds safe limits during mining, it is regarded as dangerous. The gas concentration reflects the safety of a working face, and the gas concentration in the working face varies with the advance of the working face. Over time, a control chart for gas concentration in a working face can be plotted. By analyzing the control chart, it can be determined whether gas in the working face was under control or not.

Normal Test on Sample Data

Owing to the gas concentration in the upper corner in the working face being influenced by various factors including geological conditions, conditions in the coal seams, and production conditions, the gas concentration in the working face is a random variable. The average gas concentration in the working face can better reflect the controllability of gas in the working face. Therefore, the daily average gas concentration of a working face with a sample size of 303 is computed and analyzed. In the control chart, to guarantee the effectiveness of general estimations, sample data need to undergo normal distribution testing before use.

According to the existing graphic methods used for testing the normality of data, normal distribution testing was carried out on the sample data by employing the normal probability–probability plot (P–P) and normal quantile–quantile plot (Q–Q) in SPSS17.0 software (Fig. 16). The scattered points in Q–Q and P–Q plots are all distributed at the two sides of the straight line, consistent with an oblique line; therefore, the sample data conform to the general normal distribution, which can be processed by applying an SPC control chart (Lee et al. 1998; Tan et al. 2004).
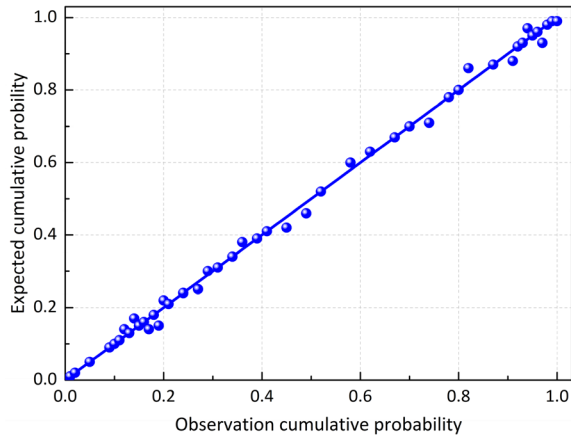
Control Chart

By processing and calculating the sample data, the parameters for the control chart calculated according to Eqs. (5) and (6) are summarized in Table 6. The control chart is shown in Fig. 17.
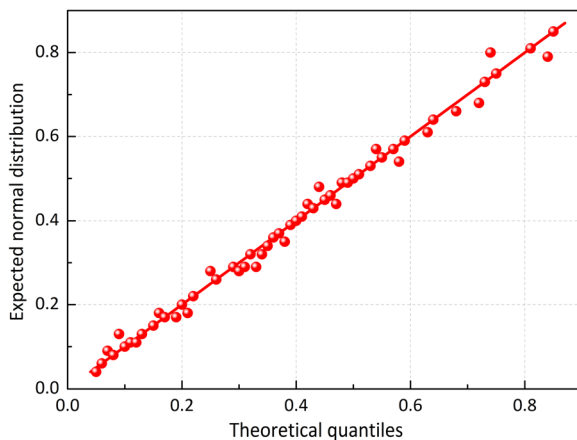
In Fig. 16, all points lie between the ranges given by UCL and LCL; that is, after undertaking GEHLB in the working face, the gas concentrations therein all remained within a controllable range. This indicates that the preventative measures against a gas accident applied to this working face were effective and feasible.

It can be seen from Fig. 17 that, in the initial stage of GEHLB, various points frequently fluctu-

ated around both sides of the CL, with a large amplitude therein. This indicated that the range of gas concentrations in the working face within the time frame was difficult to control. The reason was that, within the time frame assessed, a large amount of pressure-relief gas was accumulated in goaf. After conducting GEHLB, gas in deep goaf also flowed out at irregular intervals. After carrying out GEHLB for some time, all points clustered around the CL, implying that, within the time frame assessed, the gas concentration at the working face was easily controlled because significant volumes of pressure-relief gas had been extracted during the constant extraction of gas in goaf through the high-level boreholes. As a result, the sources of gas emission from goaf to the working face were diminished. This indicated the feasibility and efficiency of gas control measures in the working face with the given high-level borehole extraction parameters.

CONCLUSIONS

After exploring the caving of overlying strata in mine field with soft coal seams with soft roof and floor, a trapezoidal 3D model for gas migration was established. Moreover, the extraction parameters of high-level boreholes were optimized and the controllability assessment was conducted on the result (gas concentration in the working face) of extracting gas based on in situ high-level boreholes. The following conclusions were reached:

After whitening the observed surface of the established physical similarity model, the development and coalescence of fractures can be seen during excavation testing. According to the state of development of the fractures, whether overlying strata are about to be fractured or caved can be judged, which was of benefit when conducting physical similarity model tests. After the eighth periodic weighting, overlying strata in goaf remained stable during mining. The average weighting span of the working face was 8 m, and the largest height of the caving zone in goaf was 16 m, with a breaking

(a) Normal P–P plot of gas concentrations

(b) Normal Q–Q plot of gas concentrations

Figure 16. Normal plots of gas concentrations in the working face.

Table 6. Parameters required for a control chart

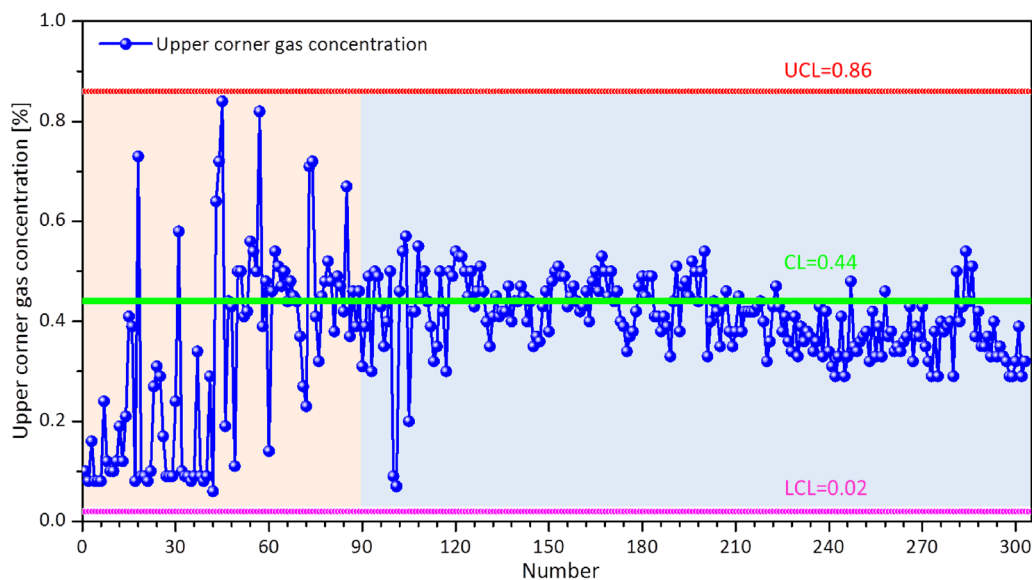| Parameter	Average	Standard deviation (δ)	CL	UCL	LCL
Value	0.44%	0.14	0.44%	0.86%	0.02%

Figure 17. Control chart of daily average gas concentration in the working face.

angle of 63°. Moreover, zones with fractures in overlying strata were partitioned upon completion of mining operations.

According to characteristics of geometric shapes of caved overlying strata and engineering conditions of the working face, a trapezoidal 3D model for gas migration was established. On this basis, numerical calculation was carried out on the model for gas migration without GEHLB, with gas extraction based on high-level boreholes with different diameters or with different negative pressures. When not carrying out GEHLB, the maximum gas concentration in goaf was 53.10%: the maximum gas concentration in goaf was negatively correlated with the diameter of high-level borehole installed. By considering the stability of boreholes and construction conditions, the optimal diameter of high-level boreholes was found to be 0.153 m. The maximum gas concentration in goaf also showed a negative correlation with the negative pressure in each borehole during gas extraction; however, the change in extraction effect was insignificant when increasing the pressure. Moreover, considering spontaneous combustion tendencies in such coal seams (and economic factors), the negative pressure applied to high-level boreholes during extraction was set to 20 kPa. Given such extraction parameters, it can be seen from the nephogram that the extraction effect was significant.

In the working face, 13 high-level drill sites were distributed, and the total amount of accumulated extracted gas was 4.582×10^5 m^3. The gas concentration never exceeded the safe limits during production in the mine. An SPC control chart showed that, after undertaking GEHLB, the gas concentrations were all between the range of control enclosed by the UCL and LCL. This indicated that the gas concentration was under control and also validated the feasibility and effectiveness of gas prevention measures implemented with these extraction parameters.

ACKNOWLEDGMENTS

REFERENCES

Bersimis, S., Psarakis, S., & Panaretos, J. (2007). Multivariate statistical process control charts: An overview. *Quality and Reliability Engineering International, 23*(5), 517–543.

Borisenko, A. (1985). Effect of gas pressure on stresses in coal strata. *Soviet Mining, 21*(1), 88–92.

Brune, J. F., & Saki, S. A. (2017). Prevention of gob ignitions and explosions in longwall mining using dynamic seals. *International Journal of Mining Science and Technology, 27*(6), 999–1003.

Chen, H., Qi, H., Long, R., & Zhang, M. (2012). Research on 10-year tendency of China coal mine accidents and the characteristics of human factors. *Safety Science, 50*(4), 745–750.

Chen, W. (2005). The costs of mitigating carbon emissions in China: Findings from China MARKAL-MACRO modeling. *Energy Policy, 33*(7), 885–896.

Chen, W., Yin, X., & Zhang, H. (2016). Towards low carbon development in China: A comparison of national and global models. *Climatic Change, 136*(1), 95–108.

Cheng, J., Li, S., Zhang, F., Zhao, C., Yang, S., & Ghosh, A. (2016). CFD modelling of ventilation optimization for improving mine safety in longwall working faces. *Journal of Loss Prevention in the Process Industries, 40,* 285–297.

Chu, T., Zhou, S., Xu, Y., & Zhao, Z. (2011). Research on the coupling effects between stereo gas extraction and coal spontaneous combustion. *Procedia Engineering, 26,* 218–227.

Enever, J., & Hennig, A. (1997). The relationship between permeability and effective stress for Australian coals and its implications with respect to coalbed methane exploration and reservoir modelling. In *1997 International Coalbed Methane Symposium*, May 12–17, 1997, Bryant Conference Center, University of Alabama, Tuscaloosa, AL.

Fan, Y., & Xia, Y. (2012). Exploring energy consumption and demand in China. *Energy, 40*(1), 23–30.

Gawuga, J. K. (1979). Flow of gas through stressed carboniferous strata. Doctoral dissertation, University of Nottingham.

Guo, H., Qu, Q., & Adhikary, D. (2017). Overburden response to longwall mining. In S. S. Peng (Ed.), *Advances in coal mine ground control* (pp. 111–155). Sawston: Woodhead Publishing.

Guo, H., Todhunter, C., Qu, Q., & Qin, Z. (2015). Longwall horizontal gas drainage through goaf pressure control. *International Journal of Coal Geology, 150,* 276–286.

Harpalani, S. (1985). *Gas flow through stressed coal*. Berkeley (USA): California University.

Hou, Z., Wundram, L., Meyer, R., Schmidt, M., Schmitz, S., & Were, P. (2012). Development of a long-term wellbore sealing concept based on numerical simulations and in situ-testing in the Altmark natural gas field. *Environmental Earth Sciences, 67*(2), 395–409.

Hu, G., Xu, J., Zhang, F., Zhao, C., Qin, W., & Zhu, Y. (2015). Coal and coalbed methane co-extraction technology based on the ground movement in the Yangquan coalfield, China. *Energies, 8*(7), 6881–6897.

Hu, G. Z., Wang, H. T., Tan, H. X., Fan, X. G., & Yuan, Z. G. (2008). Gas seepage equation of deep mined coal seams and its application. *Journal of China University of Mining and Technology, 18*(4), 483–487.

Hu, Q. T., Liang, Y. P., & Liu, J. Z. (2007). CFD simulation of goaf gas flow patterns. *Journal of China Coal Society, 32*(7), 719–723.

Hu, Q., Liang, Y., Wang, H., Zou, Q., & Sun, H. (2017). Intelligent and integrated techniques for coalbed methane (CBM) recovery and reduction of greenhouse gas emission. *Environmental Science and Pollution Research, 24*(21), 17651–17668.

Karacan, C. Ö., Esterhuizen, G. S., Schatzel, S. J., & Diamond, W. P. (2007). Reservoir simulation-based modeling for characterizing longwall methane emissions and gob gas venthole production. *International Journal of Coal Geology, 71*(2–3), 225–245.

Karacan, C. Ö., Ruiz, F. A., Cotè, Michael, & Phipps, S. (2011). Coal mine methane: A review of capture and utilization practices with benefits to mining safety and to greenhouse gas reduction. *International Journal of Coal Geology, 86*(2–3), 121–156.

Keim, S. A., Luxbacher, K. D., & Karmis, M. (2011). A numerical study on optimization of multilateral horizontal wellbore patterns for coalbed methane production in Southern Shanxi Province, China. *International Journal of Coal Geology, 86*(4), 306–317.

Khodot, V. V. (1980). Role of methane in the stress state of a coal seam. *Soviet Mining, 16*(5), 460–466.

Lau, H. C., Li, H., & Huang, S. (2017). Challenges and opportunities of coalbed methane development in China. *Energy & Fuels, 31*(5), 4588–4602.

Lee, J., Woo, J., & Rhee, S. (1998). A transformed quantile–quantile plot for normal and bimodal distributions. *Journal of Information and Optimization Sciences, 19*(3), 305–318.

Li, D. Y., Hu, C. R., & Xiong, Z. J. (2012). Gas flowing model of mining face and solve it using COMSOL. *Journal of China Coal Society, 37*(6), 967–971.

Li, Q., Lin, B., Yang, W., Zhai, C., & Hao, Z. (2011). Gas control technology and engineering practice for three-soft coal seam with low permeability in XuanGang region, China. *Procedia Engineering, 26,* 560–569.

Li, Q., Lin, B., & Zhai, C. (2015). A new technique for preventing and controlling coal and gas outburst hazard with pulse hydraulic fracturing: A case study in Yuwu coal mine, China. *Natural Hazards, 75*(3), 2931–2946.

Li, S. G., Lin, H. F., Zhao, P. X., Xiao, P., & Pan, H. Y. (2014). Dynamic evolution of mining fissure elliptic paraboloid zone and extraction coal and gas. *Journal of China Coal Society, 39*(8), 1455–1462.

Li, X. (2016). *Research on numerical simulation about double porosity model of coal seam and gas migration in goaf*. PhD thesis. China University of Mining & Technology, Beijing.

Lin, H., Huang, M., Li, S., Zhang, C., & Cheng, L. (2016). Numerical simulation of influence of Langmuir adsorption constant on gas drainage radius of drilling in coal seam. *International Journal of Mining Science and Technology, 26*(3), 377–382.

Liu, S., Li, X., Wang, D., Wu, M., Yin, G., & Li, M. (2019). Mechanical and acoustic emission characteristics of coal at temperature impact. *Natural Resources Research, 1*–18.

Liu, T. (1995). Influence of mining activities on mine rock mass and control engineering. *Journal of China Coal Society, 20,* 1–5.

Liu, T., Lin, B., Yang, W., Liu, T., & Zhai, C. (2017). An integrated technology for gas control and green mining in deep mines based on ultra-thin seam mining. *Environmental Earth Sciences, 76*(6), 243.

MacGregor, J. F., & Kourti, T. (1995). Statistical process control of multivariate processes. *Control Engineering Practice, 3*(3), 403–414.

Majdi, A., Hassani, F. P., & Nasiri, M. Y. (2012). Prediction of the height of destressed zone above the mined panel roof in longwall coal mining. *International Journal of Coal Geology, 98,* 62–72.

Palchik, V. (2003). Formation of fractured zones in overburden due to longwall mining. *Environmental Geology, 44*(1), 28–38.

Qian, M., Miao, X., & Xu, J. (1996). Theoretical study of key stratum in ground control. *Journal of China Coal Society, 21*(3), 225–230.

Qin, Z., Yuan, L., Guo, H., & Qu, Q. (2015). Investigation of longwall goaf gas flows and borehole drainage performance by CFD simulation. *International Journal of Coal Geology, 150,* 51–63.

Qu, Q., Xu, J., Wu, R., Qin, W., & Hu, G. (2015). Three-zone characterisation of coupled strata and gas behaviour in multi-seam mining. *International Journal of Rock Mechanics and Mining Sciences, 78,* 91–98.

Somerton, W. H., Soylemezoglu, I. M., & Dudley, R. C. (1975). Effect of stress on permeability of coal. *International Journal of Rock Mechanics and Mining Science & Geomechanics Abstracts, 12*(5/6), 129–145.

Tan, W. D., Gan, F. F., & Chang, T. C. (2004). Using normal quantile plot to select an appropriate transformation to achieve normality. *Computational Statistics & Data Analysis, 45*(3), 609–619.

Wang, F., Ren, T., Tu, S., Hungerford, F., & Aziz, N. (2012c). Implementation of underground longhole directional drilling technology for greenhouse gas mitigation in Chinese coal mines. *International Journal of Greenhouse Gas Control, 11,* 290–303.

Wang, G., Guo, Y., Du, C. A., Sun, L., Liu, Z., Wang, Y., et al. (2019a). Experimental study on damage and gas migration characteristics of gas-bearing coal with different pore structures under sorption-sudden unloading of methane. *Geofluids*. https://doi.org/10.1155/2019/7287438.

Wang, G., Xu, Y., & Ren, H. (2019b). Intelligent and ecological coal mining as well as clean utilization technology in China: Review and prospects. *International Journal of Mining Science and Technology, 29*(2), 161–169.

Wang, L., Cheng, Y. P., & Liu, H. Y. (2014). An analysis of fatal gas accidents in Chinese coal mines. *Safety Science, 62,* 107–113.

Wang, R., Tao, S., Wang, W., Liu, J., Shen, H., Shen, G., et al. (2012b). Black carbon emissions in China from 1949 to 2050. *Environmental Science and Technology, 46*(14), 7595–7603.

Wang, S., Huang, L., & Li, X. (2020). Analysis of rockburst triggered by hard rock fragmentation using a conical pick under high uniaxial stress. *Tunnelling and Underground Space Technology, 96,* 103195.

Wang, S., Li, X., & Wang, S. (2017). Separation and fracturing in overlying strata disturbed by longwall mining in a mineral deposit seam. *Engineering Geology, 226,* 257–266.

Wei, P., Guo, C., Zhao, S., Li, X., & Peng, S. (2019a). Determination of appropriate sampling depth of coalbed gas content: A case study. *Journal of Geophysics and Engineering, 16*(2), 411–422.

Wei, P., Huang, C., Li, X., Peng, S., & Lu, Y. (2019b). Numerical simulation of boreholes for gas extraction and effective range of gas extraction in soft coal seams. *Energy Science & Engineering, 7*(5), 1632–1648.

Wei, P., Liang, Y., Zhao, S., Peng, S., Li, X., & Meng, R. (2019c). Characterization of pores and fractures in soft coal from the no. 5 soft coalbed in the Chenghe mining area. *Processes, 7*(1), 13.

Xu, J. L., Qian, M. G., & Jin, H. W. (2004a). Study on "coal and coal-bed methane simultaneous extraction" technique on the basis of strata movement. *Journal of China Coal Society, 29*(2), 129–132.

Xu, J. L., Qian, M. G., & Jin, H. W. (2004b). Study and application of bed separation distribution and development in the process of strata movement. *Chinese Journal of Geotechnical Engineering-Chinese Edition, 26,* 632–636.

Xu, M. G., Wei, P., Li, S. G., & Wang, J. J. (2017). Experimental study on overburden migration and fracture evolution law of "three soft" coal seam fully mechanized working-face. *Journal of China Coal Society, 42*(S1), 122–127.

Yin, W., Fu, G., Yang, C., Jiang, Z., Zhu, K., & Gao, Y. (2017). Fatal gas explosion accidents on Chinese coal mines and the characteristics of unsafe behaviors: 2000–2014. *Safety Science, 92,* 173–179.

Zhang, J., & Bian, X. (2015). Numerical simulation of hydraulic fracturing coalbed methane reservoir with independent fracture grid. *Fuel, 143,* 543–546.

Zhang, J., & Liu, T. (1990). On depth of fissured zone in seam floor resulted from coal extraction and its distribution characteristics. *Journal of China Coal Society, 15*(2), 46–54.

Zhou, F., Xia, T., Wang, X., Zhang, Y., Sun, Y., & Liu, J. (2016). Recent developments in coal mine methane extraction and utilization in China: A review. *Journal of Natural Gas Science and Engineering, 31,* 437–458.